Changes in Molecular Structure upon Triplet Excitation of All-*trans*-Spheroidene in *n*-Hexane Solution and 15-*cis*-Spheroidene Bound to the Photo-Reaction Center from *Rhodobacter sphaeroides* As Revealed by Resonance-Raman Spectroscopy and Normal-Coordinate Analysis†

Yumiko Mukai-Kuroda, Ritsuko Fujii, Naomi Ko-chi, Tokutake Sashima,‡ and Yasushi Koyama*

Faculty of Science, Kwansei Gakuin University, Gakuen, Sanda 669-1337, Japan

Motoko Abe

Department of Domestic Science, Shoin Women's College, Obanoyama-cho, Shinohara, Nadaku, Kobe 657-0015, Japan

Ronald Gebhard, Ineke van der Hoef, and Johan Lugtenburg

Department of Chemistry, Gorlaeus Laboratories, Leiden University, 2300 BA Leiden, The Netherlands

Received: August 8, 2001; In Final Form: January 7, 2002

The S_0 and T_1 Raman spectra of all-*trans*-spheroidene and its deuterio derivatives (10-d, 12-d, 14-d, 15-d, 15′-d, 14′-d, and 15,15′-d_2) were recorded in *n*-hexane solution. The T_1 state was generated by the use of a sensitizer, anthracene. An empirical normal-coordinate analysis of the spectral data was performed by using Urey−Bradley−Shimanouchi force field; non-UBS cross terms were also introduced. By the use of each carbon−carbon stretching force constant as a scale of bond order, large changes in bond order upon triplet excitation were identified in the central part of the conjugated chain: decrease in bond order was in the order, C13═C14 > C11═C12 > C9═C10 > C15═15′, whereas increase in bond order was in the order, C12−C13 > C14−C15 ≈ C14′−C15′. In other words, the triplet-excited region where the largest changes in bond order take place was located, not at the center of the entire carbon skeleton, but at the center of the conjugated chain. The S_0 and T_1 Raman spectra of 15-*cis*-spheroidene and its deuterio derivatives (12-d, 14-d, 15-d, 15′-d, 14′-d and 15,15′-d_2) incorporated into the photoreaction center from *Rhodobacter sphaeroides* R26 were also recorded. The T_1 state of spheroidene was generated by excitation of bacteriochlorophyll at the Q_x absorption and subsequent triplet-energy transfer to the carotenoid. The S_0- and T_1-state carbon−carbon stretching force constants showed changes in bond order similar to those of all-*trans*-spheroidene in solution. However, empirical and normal-coordinate analysis of the T_1 Raman spectra showed twistings around the C15═C15′, C13═C14 and C11═C12 bonds, the values of which were temporarily estimated to be +45°, −30° and +30°, respectively. A hypothetical mechanism of triplet-energy dissipation triggered by rotational motion around those double bonds has been proposed.

Introduction

The carotenoid (Car), spheroidene, in the photoreaction center (RC) of *Rhodobacter (Rb.) sphaeroides* plays the photoprotective function (see refs 1 and 2 for reviews). When excessive light energy is supplied, the reducing conditions cause the reverse electron transfer along the L branch, and charge recombination at the special-pair BChls (P) to generate the triplet (T_1) state. To avoid sensitized generation of singlet oxygen, the triplet energy needs to be transferred to the Car, presumably via one of the accessory BChls (B_M), to be dissipated. The detailed mechanisms of the triplet-energy dissipation, in which both the Car and the apo-peptides are apparently involved, are still unknown.

The properties of the special-pair triplet (^{3}P) and the mechanisms of the triplet-energy transfer to the Car have been extensively studied (see ref 3 for a review) by means of time-resolved electronic-absorption[4−9] and EPR[10,11] spectroscopies: A unique property of the P → Car triplet-energy transfer is its strong temperature dependence; at room temperature, its efficiency is very high and only ^{3}Car (triplet carotenoid) is practically seen, whereas below 20 K, its efficiency drastically goes down and only ^{3}P is seen. The crucial role of B_M in mediating the P → Car triplet-energy transfer has been established,[7,8,11] and the activation energies of the triplet-energy transfer were determined for BChl **a** and its derivatives bound at the B_M site.[9]

A unique cis configuration of the Car was first identified in this organism by resonance-Raman spectroscopy.[12] The configuration of spheroidene in the RC from *Rb. sphaeroides* has

† Part of the special issue "Mitsuo Tasumi Festschrift".

* To whom correspondence should be addressed. E-mail: ykoyama@kwansei.ac.jp. Fax: +81-795-65-9077.

‡ Present address: Kanagawa Academy of Science and Technology (KAST), KSP Building, 3-2-1 Sakada, Takatsu-ku, Kawasaki 213-0012, Japan.

10.1021/jp0130822 CCC: $22.00
Published on Web 03/06/2002

been determined to be 15-cis by resonance-Raman,[13,14] CD[15] and NMR[16−18] spectroscopies, and by X-ray crystallography.[19,20] The distortion of the conjugated backbone of those Cars upon binding to the RCs has been identified by Raman spectroscopy.[16,21−23]

The particular 15-cis configuration has been ubiquitously found not only in the quinone-type RCs of other purple photosynthetic bacteria i.e., *Rb. sphaeroides* G1C[21] and *Rhodospirillum rubrum* S1,[24] and that of spinach PS II,[25] but also in the ion sulfur-type RCs of a green bacterium, *Chlorobium tepidum*,[26] an alga, *Synechococcus vulcanus*,[26] and spinach PS I.[27] Because the photoprotective function is expected to be most crucial in the RC, it is natural to correlate the natural selection of the 15-cis configuration, during the history of the photosynthetic organism, to this particular function, and to address a question: Why has the 15-cis configuration been selected by the RCs (see refs 2 and 28 for reviews)?

Comparison among a set of cis-trans isomers in solution may provide information concerning the unique T_1-state properties of the 15-cis configuration: A set of cis-trans isomers of β-carotene was examined by time-resolved Raman[29] and absorption[30] spectroscopies and by determination of triplet-sensitized isomerization.[31] The results indicated that the presence of extremely rapid 15-cis to all-trans isomerization in the T_1 state (the 15-cis T_1 is too short-lived to be detected) with a quantum yield of almost unity (see ref 32 for a review). Most recently, a set of cis-trans isomers of spheroidene was examined by time-resolved absorption spectroscopy and determination of the quantum yield of triplet-sensitized isomerization.[33] All the cis isomers exhibited the $T_1 \rightarrow S_0$ intersystem crossing six times faster than the all-trans isomer, and the T_1-state isomerization was the fastest in the 15-cis isomer. The results strongly suggested that the 15-cis isomer is most advantageous in dissipating the triplet energy.

The above pair of comparison of isomeric carotenoids has lead us to propose a hypothetical mechanism of triplet-energy dissipation, which includes rotation around the 15-cis bond of the RC-bound spheroidene.[23,34] The key idea behind this hypothetical mechanism is that the rotation around a carbon−carbon double bond causes a change in the orbital angular momentum around the carbon atoms, and as a result, a change in the spin angular momentum to enhance the $T_1 \rightarrow S_0$ intersystem crossing (relaxation) accompanying the triplet-energy dissipation.

The structure of the RC-bound 15-*cis*-spheroidene in the T_1 state should provide further insight into the mechanism of triplet-energy dissipation: Transient resonance-Raman spectroscopy showed that a cis configuration was retained in the T_1 state,[35] although enormous enhancement of some Raman lines strongly suggested the twisting of the conjugated backbone.[23] The twisting around the C15═C15′ cis bond seemed to support the above hypothetical mechanism. Prolonged irradiation actually caused the generation of the all-trans isomer.[23]

This mechanism has been questioned by incorporating locked-15,15′-*cis*-spheroidene (hereafter called "locked 15-*cis*-spheroidene") into the RC of *Rb. sphaeroides*:[36] locking the 15-cis configuration by introducing additional single bonds did not substantially change the decay time of the T_1 Car. This question needs to be answered before establishing the above hypothetical mechanism. In the present investigation, we have tried to extract the structural information of (unlocked) 15-*cis*-spheroidene bound to the RC from *Rb. sphaeroides*, in both the S_0 and T_1 states, by means of transient-Raman spectroscopy and normal-coordinate analysis of spheroidene and its deuterio derivatives incorporated into the RC from the *Rb. sphaeroides* R 26. The results have provided us with deeper insight into the mechanisms of triplet-energy dissipation.

The S_0 Raman spectra of d_0 and deuterio spheroidenes in solution and bound to the RC have been presented and analyzed empirically in relation to the structure of spheroidene in the S_0 state.[37] The present investigation is based on the normal-coordinate analysis of the S_0 and T_1 Raman spectra, and focuses on the T_1-state structures and the mechanisms of triplet-energy dissipation by the RC-bound Car.

Experimental Section

Sample Preparation. *(a) All-trans-Spheroidene and its Deuterio Derivatives.* All-*trans*-spheroidene of natural-abundance isotopic composition (hereafter called "d_0 spheroidene") was prepared as described previously.[38] All-*trans*-deuterio spheroidenes including 10-d, 12-d, 14-d, 14′-d, 15-d, 15′-d and 15,15′-d_2 spheroidenes were prepared by the methods described previously.[39] *(b) Preparation of the RCs from Rb. sphaeroides Containing d_0 and Deuterio Spheroidenes.* The RC containing d_0 spheroidene was prepared by (i) solubilization of the chromatophores (25 000−278 000 × *g* fraction) from *Rb. sphaeroides* 2.4.1 with LDAO in the presence of 150 mM NaCl, (ii) ammonium sulfate precipitation, and (iii) DE52 ion-exchange column chromatography using stepwise elution with 50−200 mM NaCl according to the method of Cogdell and Parson.[4,40] The RCs containing deuterio spheroidenes were obtained by their incorporation [41] into the RC from *Rb. sphaeroides* R26,[42] the spheroidene:RC ratio being 15:1. We found that iodine-sensitized photoisomerization[38] of each all-*trans*-spheroidene in advance greatly enhanced the efficiency of incorporation. The amounts of incorporation of 12-d, 14-d, 14′-d, 15-d, 15′-d, and 15,15′-d_2 spheroidenes into the RC for S_0/T_1 Raman measurements were 98/98, 78/88, 78/88, 76/85, 87/82, and 80/86%, respectively.

Raman Measurements. *(a) S_0 Raman Measurements.* The Raman spectra of d_0 and deuterio all-*trans*-spheroidenes in the S_0 state were recorded in *n*-hexane solution ($0.2-5.0 \times 10^{-4}$ M) at liquid nitrogen temperature by the use of the CW 488.0 nm line (7−14 mW) of an Ar^+ laser (Lexel 95) and a Raman spectrometer (JASCO TRS-300) equipped with an image-intensified diode-array detector (Princeton Instruments IRY-700). The Raman spectrum of d_0 and deuterio spheroidenes incorporated into the RC from *Rb. sphaeroides* R26 was measured by the use of the CW 514.5 nm line, instead. No spectral smoothing was performed. The Raman frequencies were calibrated against those of acetone, benzene, ethyl acetate, *n*-hexane, and toluene.

(b) T_1 Raman Measurements. The Raman spectra of d_0 and deuterio all-*trans*-spheroidenes in *n*-hexane solution ($1.3-5.0 \times 10^{-5}$ M) were recorded in the presence of a triplet sensitizer, anthracene (60−100 fold), by the use of a pump−probe technique described previously[29] with the following modifications: The 355 nm pulses (power 5.0 mJ/pulse, duration 6 ns, and repetition 10 Hz) from a Nd:YAG laser (Lumonics HY-400) were used for pumping, whereas the 532 nm pulses (2 mJ/pulse, 5 ns and 10 Hz) from a Nd:YAG laser (Spectron SL284G) were used for probing. The pump and probe pulses coaxially irradiated a flat jet stream of the sample solution from an angle of 45°, and 90° Raman scattering was collected. The delay time between the pump and probe pulses was set to be 1.0 μs by the use of a high-voltage pulse generator (Princeton Instruments, FG-100). The Raman scattering was detected by the above image-intensified diode-array detector, which was

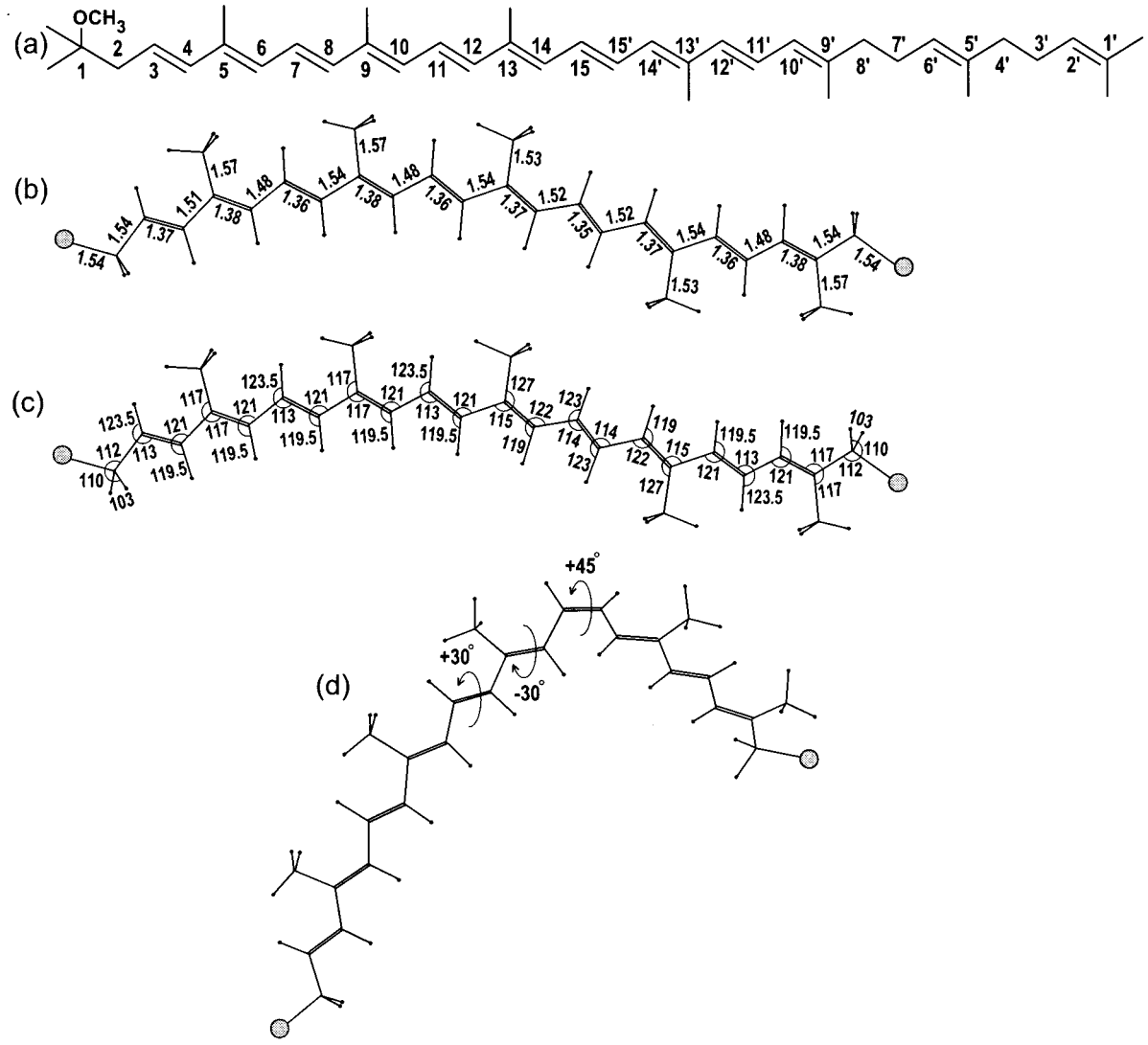

Figure 1. Chemical structure and models of spheroidene: (a) Chemical structure and the numbering of skeletal carbon atoms of spheroidene, (b) the bond lengths and (c) the bond angles of the model used for the normal-coordinate analysis of all-*trans*-spheroidene in solution, and (d) the twistings of the conjugated backbone of the model used for the normal-coordinate analysis of T_1 15-*cis*-spheroidene bound to the RC (the same bond lengths and bond angles as the model of all-*trans*-spheroidene were assumed). Twisting around the C15═C15′ bond by 30° alone was assumed in the S_0 state (not shown).

gated for 3.5 μs by the use of a delay-pulse generator (Stanford Research Systems DG-535). A T_1 Raman spectrum was obtained as a difference spectrum of "with pump" minus "without pump" after subtracting the Raman lines of the solvent, *n*-hexane, from each spectrum. For the T_1 Raman spectra of 10-d, 12-d, 14-d, 15-d, 15′-d spheroidenes, spectral smoothing was performed. The purity of each sample examined by HPLC using a detection wavelength of 450 nm, before/after the T_1 Raman measurement, was as follows: d_0, 97/95; 10-d, 100/-; 12-d, 100/91; 14-d, 88/75; 14′-d, 62/54; 15-d, 80/74; 15′-d, 75/60; 15,15′-d_2, 99/87%.

The Raman spectra of d_0 spheroidene in wild-type RC and deuterio spheroidenes incorporated into carotenoidless RC were recorded by the method of Ohashi et al.[23] except for the following modifications due to the limited amounts of deuterio spheroidenes: the sample concentrations were reduced to OD_{800} 11−18 cm^{-1}, and the power of pump pulses (600 nm, 5 ns and 10 Hz) and that of probe pulses (532 nm, 6 ns and 10 Hz) were increased to 3.0 mJ/pulse and 0.75−1.5 mJ/pulse, respectively.

Normal-Coordinate Analysis. Figure 1a shows the entire chemical structure of all-*trans*-spheroidene, and Figure 1b−d shows the models of all-*trans*- and 15-*cis*-spheroidenes that were used for normal-coordinate analyses. One peripheral group beyond C1 and the other peripheral group beyond C7′ were truncated, and replaced by a pair of mass units of 15. The bond lengths and the bond angles concerning the carbon skeleton were estimated based on the structure of β-carotene determined by X-ray crystallography;[43] the methyl and olefinic C−H bond lengths were set to be 1.095 and 1.08 Å, respectively. Completely planar conformations were assumed for the all-trans isomer in solution in both the S_0 and T_1 states. For the 15-cis isomer bound to the RC, the C15═C15′ bond was twisted by +30° in the S_0 state, whereas the C15═C15′, C13═C14 and C11═C12 bonds were twisted by +45°, −30° and +30°, respectively, in the T_1 state (vide infra).

In the present normal-coordinate analyses, we used Urey−Bradley−Shimanouchi (UBS) force field expressed by the force constants of stretching (*K*), bending (*H*), nonbonded repulsion (*F*), intramolecular resistance force (κ), wagging (*W*), and torsion (*T*). Non-UBS cross terms including the stretching-stretching (*k*), bending−bending (*h*), and wagging−wagging (*w*) cross terms were also introduced. In 15-*cis*-spheroidene, additional cross terms (*kh*) between (1) the C14−C15 and C14′−C15′

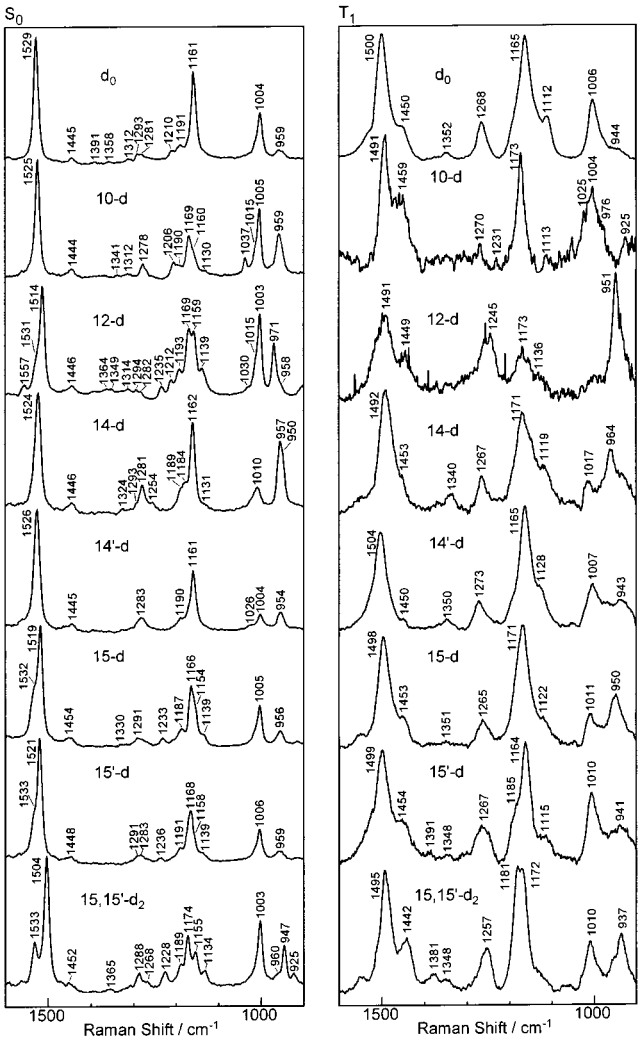

Figure 2. S_0 Raman spectra (488 nm probe) and the T_1 Raman spectra (532 nm probe) of d_0 and various deuterio all-*trans*-spheroidenes in *n*-hexane solution. The T_1 state of spheroidene was generated by excitation of anthracene (sensitizer) at 355 nm and subsequent triplet-energy transfer to the Car.

stretchings and (2) the C14−H, C15−H and C15′−H bendings within the 15-cis bend were introduced. The Normal vibrations were calculated by Wilson's GF-matrix method [44] using programs BGLZ, LSMB, and LXZ originally written in Prof. Takehiko Shimanouchi's laboratory.[45]

Results

Empirical Assignments of the S_0 and T_1 Raman Lines of d_0 Spheroidenes Based on Deuteration Effects. *(a) All-trans-Spheroidene in Solution.* Figure 2 shows the Raman spectra of all-*trans*-spheroidene in *n*-hexane solution in both the S_0 and the T_1 states. Table 1a summarizes a set of empirical assignments for the S_0 and T_1 Raman lines of d_0 all-*trans*-spheroidene, the details of which will be described below according to the following order of appearance in the spectral region of 1600−900 cm^{-1}: (1) the C═C stretchings (1600−1500 cm^{-1}), (2) the methyl in-plane (ip) asymmetric and symmetric deformations (∼1450 and 1390 cm^{-1}, respectively), (3) the C−H ip bendings (1300−1250 cm^{-1}), (4) the C−C stretchings (1250−1100 cm^{-1}), (5) the methyl ip rockings (1010−1000 cm^{-1}), and (6) the C−H out-of-plane (op) waggings (960−940 cm^{-1}). (Hereafter, we will omit "ip" and "op" except when they are necessary.) Those vibrational modes in which the displacements of atoms are in accord with those upon the $1^1B_u^+ \leftarrow 1^1A_g^-$ (∼480 nm) and the $n^3A_g^+ \leftarrow 1^3B_u^+$ (∼505 nm) π-π^* transitions should give rise to strong or medium resonance-Raman lines in the S_0 and T_1 states when probed at 488 and 532 nm, respectively. Thus, all the observed Raman lines are ascribable to the normal modes which are associated with the conjugated chain.

TABLE 1: Frequencies and Empirical Assignments of the S_0 and T_1 Raman Lines for (a) d_0 All-*trans*-Spheroidene in *n*-Hexane Solution and (b) d_0 15-*cis*-Spheroidene Bound to the RC

(a)	S_0 state	T_1 state	
frequency	assignment	frequency	assignment
1529	central C═C str	1500	C11═C12, C13═C14 str
1445	Me asym def	1450	Me asym def
1391	Me sym def	1352	Me sym def
1312			
1293	C11−H, C11′−H bend		
1281		1268	C10−H, C12−H bend
1210	C12−C13, C12′−C13′ str		
1191	C8−C9 str	1165	C10−C11, C14−C15 str
1161	C10−C11str / C14−C15, C14′−C15′ str	1112	C10−C11 ∼ C14′−C15′ str
1004	Me rock	1006	13Me rock
959	C−H wag	944	C−H wag

(b)	S_0 state	T_1 state	
frequency	assignment	frequency	assignment
1534	C11═C12, C13═C14, C13′═C14′ str	1526	C11═C12 str
(1532)	C15═C15′ str	1505	C13═C14, C15═C15′ str
1445	Me asym def		
1288	C11−H, C11′−H bend	1335	C15−H, C15′−H bend
1239	C15−H, C15′−H bend		
1212	C12−C13, C12′−C13′ str		
1190	C8−C9 str		
1168	C14−C15 str	1182	C10−C11 str
1159	C10−C11 str	1156	C14−C15 str
1001	Me rock	1008	13Me rock
973	C−H wag		
954	C−H wag	935	C−H wag

Spectral changes upon deuteration are useful in assigning the Raman lines of d_0 spheroidene: In a planar conjugated chain, an ip C−H bending vibration can couple with the C═C stretching and the C−C stretching vibrations appearing on the higher- and the lower-frequency-sides, and as a result, push (through the coupling) the former to the higher frequencies and the latter to the lower frequencies. Upon replacement of an olefinic proton by a deuterium, the above coupling is removed (the C−D bending vibration shifts all the way down to below 950 cm^{-1}), and the low-frequency-shift (high-frequency-shift) of the relevant C═C (C−C) stretching Raman line takes place. Therefore, the deuteration of each olefinic H facilitates assignments of the coupled C═C and C−C stretchings. It is to be noted that all the C═C and C−C stretchings and the C−H bendings, which take place within a planar polyene skeleton terminated by a pair of methyl groups on both ends, can couple with one another. This type of coupling among ip modes is also useful to probe the planarity of the conjugated chain.

Assignments of the S_0 Raman Lines. (1) The strongest Raman line at 1529 cm^{-1} can be assigned to a set of C═C stretchings coupled in-phase (the a_g-type mode). The low-frequency shifts upon the 10-d, 12-d, 14-d, 15-d, 14′-d, and 15′-d substitutions

are 4, 15, 5, 10, 3, and 8 cm^{-1}, respectively. The results suggest that the stretchings of the double bonds in the central part of the conjugated chain are coupled with one another (see Figure 1). Similar shifts upon the 14-d and 14′-d substitutions (5 and 3 cm^{-1}) as well as those upon the 15-d and 15′-d substitutions (10 and 8 cm^{-1}) strongly suggest that the atomic displacements in this particular mode are symmetric with respect to the C15═C15′ bond. (2) The 1445 and 1391 cm^{-1} Raman lines can be assigned to the methyl asymmetric and symmetric deformations, respectively, based on their frequency and intensity. (3) A pair of weak but distinct Raman lines at 1293 and 1281 cm^{-1} can be associated with the C11—H and C11′—H bendings, because they change spectral patterns substantially upon the 10-d and 12-d substitutions, but very little upon other deuterations. (4) It was shown, in all-*trans*-*β*-carotene, that the stretching between the methylated and unmethylated carbon atoms in the conjugated chain is higher in frequency than that between a pair of unmethylated carbon atoms.[46,47] The weak 1210 cm^{-1} Raman line splits into two components upon the 12-d substitution; one component upshifts to 1235 cm^{-1} and the other component stays at 1212 cm^{-1}. Upon the 14-d and 14′-d substitutions, it shifts to as high as to be overlapped with the C11—H bending Raman lines mentioned above (∼1280 cm^{-1}). Therefore, the 1210 cm^{-1} Raman line can be assigned to an overlap of coupled vibrations, i.e., one, the C12—C13 stretching which is coupled with the C12—H and C14—H bendings and the other, the C12′—C13′ stretching which is coupled with the C12′—H and C14′—H ip bendings. The other weak 1191 cm^{-1} Raman line shifts to 1278 cm^{-1} upon the 10-d substitution, but no clear spectral changes are seen upon other deuterations. Therefore, the Raman line can be assigned to the C8—C9 stretching coupled with the C10—H bending. It was also shown[46,47] that the C—C stretchings coupled in-phase taking place in the central part of a long conjugated chain give rise to strong resonance-Raman lines: The second strongest Raman line at 1161 cm^{-1} splits into a peak at 1169 cm^{-1} and a shoulder at 1160 cm^{-1} upon the 10-d substitution, and widely splits into a pair of Raman lines at 1169 and 1159 cm^{-1} upon the 12-d substitution. The results indicate a strong contribution of the C10—C11 stretching (which can couple with the C10—H and the C12—H bendings) to this Raman mode. Upon the 15-d and 15′-d substitutions, a part of this 1161 cm^{-1} Raman line seems to upshift to 1233 and 1236 cm^{-1}, respectively, and the remaining component splits into two components (1166 and 1154 cm^{-1} and 1168 and 1158 cm^{-1}, respectively). This indicates the contribution of the C14—C15 and the C14′—C15′ stretchings as well; similar spectral changes upon the 15-d and 15′-d substitutions indicate that the atomic displacements in this particular mode are symmetric with respect to the C15═C15′ bond. (5) The strong 1004 cm^{-1} Raman line can be assigned to the methyl rocking vibration based on its frequency and intensity referring to the cases of all-*trans*-*β*-carotene[46,47] and all-*trans*-retinal.[48] (6) The 959 cm^{-1} Raman line can be assigned to a C—H wagging vibrations coupled with the C═C torsion.

Assignments of T_1 Raman Lines. (1) The strongest Raman line at 1500 cm^{-1} can be assigned to the C═C stretchings localized on the C11═C12 and C13═C14 bonds. It shifts to 1491 cm^{-1} upon both the 10-d and 12-d substitutions, a fact which indicates the contribution of the C11═C12 stretching. The downshifts of this Raman line upon the 14-d and 15-d substitutions (−8 and −2 cm^{-1}) are larger than those upon the 14′-d and 15′-d substitutions (+4 and −1 cm^{-1}), a fact which indicates a contribution of the C13═C14 stretching rather than that of the C13′═C14′ stretching. (2) The 1450 cm^{-1} Raman line on the shoulder and the weak 1352 cm^{-1} Raman line can be assigned to the methyl asymmetric and symmetric deformations, respectively. (3) A Raman line at 1268 cm^{-1} can be associated with the C—H ip bendings. Apparent changes in the Raman line upon the 10-d and 12-d substitutions suggest the contributions of the C10—H and C12—H bendings. (4) The strong 1165 cm^{-1} Raman line can be assigned to a vibration in which the C10—C11 and C14—C15 stretchings are coupled with each other, because it substantially upshifts upon the 10-d (8 cm^{-1}), 12-d (8 cm^{-1}), 14-d (6 cm^{-1}) and 15-d (6 cm^{-1}) substitutions, but hardly affected by the 14′-d and 15′-d substitutions. The medium 1112 cm^{-1} Raman line on the shoulder that upshifts upon the 12-d, 14-d, 15-d, 15′-d, and 14′-d substitutions (6, 24, 7, 10, 3, and 16 cm^{-1}, respectively) can be assigned to a delocalized coupled mode extending the entire region from the C10—C11 to the C14′—C15′ bond. (5)(6) The 1006 cm^{-1} and the 944 cm^{-1} Raman lines can be assigned to the methyl ip rocking and the C—H wagging vibrations, respectively, as in the case of the S_0 state.

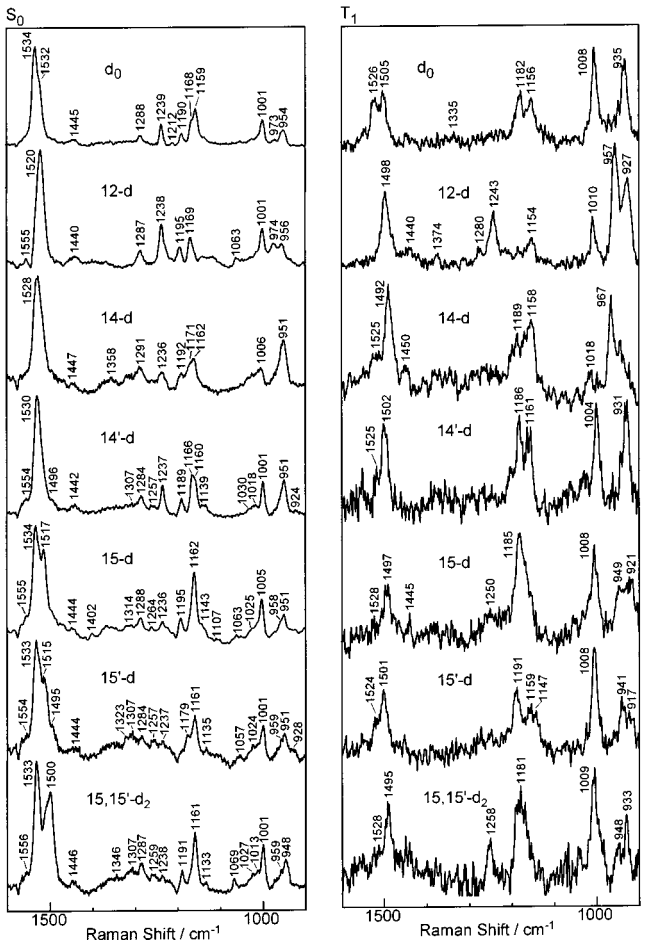

Figure 3. S_0 Raman spectra (514.5 nm probe) and the T_1 Raman spectra (532 nm probe) of d_0 and various deuterio 15-*cis*-spheroidenes bound to the RC. The T_1 state of spheroidene was generated by excitation of bacteriochlorophyll at 600 nm and subsequent triplet-energy transfer to the Car.

(b) 15-cis-Spheroidene Bound to the RC. Figure 3 shows the Raman spectra of 15-*cis*-spheroidene bound to the RC in both the S_0 and T_1 states. Table 1b summarizes a set of empirical assignments, the details of which will be described below. *Assignment of the S_0 Raman lines.* (1) The strongest Raman profile above 1530 cm^{-1} can be regarded as an overlap of two components: One at 1534 cm^{-1} is a coupled mode of the C11═C12, C13═C14 and C13′═C14′ stretchings that

downshift upon the 12-d, 14-d and 14′-d substitutions to 1520, 1528 and 1530 cm^{-1}, respectively, because of decoupling from the C12−H, C14−H and C14′-H bendings. The other at 1532 cm^{-1} is the C15═C15′ stretching that downshifts upon the 15-d, 15′-d and 15,15′-d_2 substitutions to as low as 1517, 1515 and 1500 cm^{-1} because of decoupling from the C15−H and C15′-H bendings. (2) The 1445 cm^{-1} Raman line can be assigned to the methyl asymmetric deformation as in the case of d_0 all-*trans*-spheroidene. (3) The weak 1288 cm^{-1} Raman line which is not so affected by all the present deuterium substitutions can be temporarily associated with the C11−H and C11′−H bendings (no 11-d or 11′-d spheroidenes are now available). The medium Raman line at 1239 cm^{-1} can be assigned to the key Raman line of the 15-cis configuration that has been identified in β-carotene[46,47] and other carotenoids.[28] It is due to the C15−H and C15′−H ip bendings coupled with the C15═C15′ stretching in the 15-cis configuration. It is almost unaffected by the 12-d, 14-d and 14′-d substitutions, but substantially decreased in intensity upon the 15-d, 15′-d and 15,15′-d_2 substitutions (the remaining component may be due to another normal mode). (4) A pair of weak Raman lines at 1212 and 1190 cm^{-1} can be assigned to the C12−C13 and the C8−C9 stretchings as in the case of d_0 all-*trans*-spheroidene. One of the medium Raman lines at 1168 cm^{-1}, which is unaffected by the 12-d, 14-d, and 14′-d substitutions but disappears upon the 15-d and 15,15′-d_2 substitutions, can be assigned to the C14−C15 stretching coupled with the C15−H bending. The other medium Raman line at 1159 cm^{-1}, which disappears upon the 12-d substitution and remains unaffected upon other deuterium substitutions, can be assigned to the C10−C11 stretching. (5)(6) The 1001 cm^{-1} Raman line can be assigned to the methyl ip rockings, whereas the 973 and 954 cm^{-1} Raman lines to the C−H waggings.

Assignments of T_1 Raman lines. (1) A pair of strong Raman lines appear in the C═C stretching region: The 1526 cm^{-1} Raman line, which disappears upon the 12-d substitution but remains with reduced intensity in other deuterium substitutions, can be assigned to the C11═C12 stretching coupled with the C12−H deformation. The other 1505 cm^{-1} Raman line which downshifts by 13 and 8 cm^{-1} upon the 14-d and 15-d substitutions can be associated with the C13═C14 and C15═C15′ stretchings coupled with the relevant C−H bendings. The contribution of the C13═C14 stretching and the C14−H bending may be the strongest. (2)(3) None of the methyl deformation and the C−H bending modes appear in the spectrum. (4) Another pair of strong Raman lines appears in the C−C stretching region: The 1182 cm^{-1} Raman line, which disappears upon the 12-d substitution but remains in a similar frequency region upon other substitutions (as a higher-frequency component) can be assigned to the C10−C11 stretching. The 1156 cm^{-1} Raman line, which disappears upon the 15-d and 15,15′-d_2 substitutions but remains unaffected by other deuterations, can be assigned to the C14−C15 stretching.

Unique features of the T_1 Raman spectrum of the RC-bound 15-*cis*-spheroidene is the enormous intensity enhancement of the methyl rocking and the C−H wagging Raman lines as well as the disappearance of the methyl deformation and the C−H bending Raman lines. This strongly suggests a substantial twisting of the conjugated chain upon the $T_n \leftarrow T_1$ transition. The disappearance of the key Raman line of the 15-cis configuration at 1239 cm^{-1} and the appearance of a weak feature around 1335 cm^{-1} suggest the presence of substantial twisting around the C15═C15′ bond upon triplet excitation of the RC-bound spheroidene (vide infra).

Sets of assignments for various deuterio spheroidenes of the S_0 and T_1 Raman lines for the all-trans isomer in *n*-hexane solution and the 15-cis isomer bound to the RC have also been obtained (data not shown).

Normal-Coordinate Analyses. *(a) All-trans-Spheroidenes in Solution. Determination of Force Constants in the S_0 and T_1 States.* The S_0-state force constants were determined as follows: A set of force constants determined by Saito and Tasumi[46] for all-*trans*-β-carotene was initially transferred (force constants in the peripheral parts were transferred from other molecules). Then, most of the UBS force constants and non-UBS cross terms were adjusted to fit the frequencies and the empirical assignments of the observed Raman lines of all the d_0 and deuterio spheroidenes. The fixed and adjusted force constants are shown in Table 2 in Roman and italic, respectively. No attempts were made either to fit the frequencies of the methyl deformations and rockings or to fit those of the C−D bendings. The L_x matrix showing the replacements of atoms was used to choose those normal modes which are supposed to give rise to resonance-Raman intensity; in particular, extended skeletal modes taking place in the central part of the conjugated chain were selected as strongly-Raman active modes. The number of observed Raman lines used for fitting was 71, whereas the number of force constants determined was 57.

In the T_1 state, only the C9═C10, C10−C11, C11═C12, C12−C13, C13═C14, C14−C15, C15═C15′, and C14′−C15′ stretching force constants and the relevant stretching-stretching and bending-bending cross terms were adjusted because of the limited number of deuterio species and observed Raman lines. The rest of the force constants was assumed to be the same as those in the S_0 state. Here again, the adjustment of those force constants was performed to fit the calculated frequencies and Raman-active normal modes to the observed frequencies and the empirical assignments for all the d_0 and deuterio spheroidenes.

Table 2 lists the S_0 and T_1 force constants which have been determined as the results of the above normal-coordinate analysis (shown in italic). Figure 4 compares the observed and the calculated frequencies for d_0 and various deuterio all-*trans*-spheroidenes. Agreement between the observed and the calculated frequencies are satisfactory in both the S_0 and T_1 states with the exception of those of the C−D bendings whose frequencies were not adjusted at all (below around 950 cm^{-1}). Thus, the C═C and the C−C stretching force constants determined are considered to be reliable enough to use as a scale of the carbon−carbon bond orders (vide infra).

Normal Modes in the S_0 and T_1 States. Table 3a lists the calculated frequencies and the normal modes of d_0 all-*trans*-spheroidene in solution in both the S_0 and T_1 states. (Those of various deuterio all-*trans*-spheroidenes are shown in Table 1S of "Supporting Information available".) Each normal mode has been characterized in the table by referring to both the potential energy distribution (p.e.d.) and the L_x matrix. The empirical assignments based on the apparent changes in the spectral pattern upon various deuterations (Table 1a) are now confirmed, in general, and the normal modes have been more specifically determined by the present normal-coordinate analysis.

Close examination of Table 3a reveals that the normal modes in the S_0 state tend to be symmetric with respect to the C15═C15′ bond, whereas those in the T_1 state tend to be localized on the left-hand-side of the molecule shown in Figure 1a: In the S_0 state, the 1445 cm^{-1} Raman line is assigned to the 13Me and 13′Me asymmetric deformations, and the 1004 cm^{-1} Raman line to the 13Me and 13′Me rockings; each pair

TABLE 2: S_0 and T_1 Force Constants for All-*trans*-Spheroidene in *n*-Hexane Solution

	S_0	T_1		S_0	T_1		S_0	T_1
Urey−Bradley−Shimanouchi (UBS) force constants[a]								
K(Dy−C)	*3.50*		*K*(14−15)	*4.32*	*4.37*	*W*(HCC3=C)	0.335	
K(2−3)	*3.80*		*K*(15=15′)	*5.72*	*5.60*	*W*(HCC4=C)	0.335	
K(3=4)	*6.70*		*K*(14′−15′)	*4.32*	*4.38*	*W*(HCC6=C)	0.335	
K(4−5)	*3.90*		*K*(13′=14′)	*6.00*		*W*(HCC7=C)	0.335	
K(5=6)	*6.60*		*K*(12′−13′)	*4.32*		*W*(HCC8=C)	0.335	
K(6−7)	*3.90*		*K*(11′=12′)	*6.11*		*W*(HCC10=C)	0.33	
K(7=8)	*6.50*		*K*(10′−11′)	*4.00*		*W*(HCC11=C)	0.27	
K(8−9)	*3.95*		*K*(9′=10′)	*6.35*		*W*(HCC12=C)	0.33	
K(9=10)	*6.35*	*6.00*	*K*(8′−9′)	*3.80*		*W*(HCC14=C)	0.335	
K(10−11)	*4.31*	*4.32*	*K*(C−Me)	2.70		*W*(HCC15=C)	0.255	
K(11=12)	*6.06*	*5.45*	*K*(=CH) o	4.50		*W*(HCC15′=C)	0.255	
K(12−13)	*4.32*	*4.59*	*K*(−CH) me	4.27		*W*(HCC14′=C)	0.335	
K(13=14)	*5.95*	*5.30*	*K*(−CH) met	*4.20*		*W*(HCC12′=C)	0.33	
						W(HCC11′=C)	0.27	
H(C−C=C)	0.24		*F*(C−C=C)	0.34		*W*(HCC10′=C)	0.33	
H(C−C−C)	0.23		*F*(C−C−C)	0.40		*W*(MeCC=C)	0.335	
H(C=C−H)	*0.205*		*F*(C=C−H)	0.48				
H(C−C−H) o[c]	0.20		*F*(C−C−H) o	0.41		*T*(C=C)	0.49	*0.462*
H(C−C−H) me[d]	0.24		*F*(C−C−H) me	0.55		*T*(C−C)	0.09	
H(H−C−H) me	0.36		*F*(H−C−H) me	*0.195*		*T*(C−Me)	0.047	
H(Dy−C−C)	*0.20*		*F*(Dy−C−C)	*0.40*				
H(Dy−C−H)	*0.19*		*F*(Dy−C−H)	*0.40*				
H(C−C−H) met[e]	*0.19*		*F*(C−C−H) met	*0.40*		κ me	−0.04	
H(H−C−H) met	*0.40*		*F*(H−C−H) met	*0.10*		κ met	−0.04	
non-UBS force constants[b]								
k(3=4)(5=6)	*−0.45*		*k*(14−15)(12′−13′)	*−0.10*	*0.50*	*k*(C=C)(C−C) long[f]	*0.03*	*0.04*
k(5=6)(7=8)	*−0.45*		*k*(Dy−C)(C−C)	*−0.15*		*k*(C=C)(C−Me)	*0.30*	
k(7=8)(9=10)	*−0.45*		*k*(2−3)(3=4)	*0.27*		*k*(C=C)(13−Me)	0.20	
k(9=10)(11=12)	*−0.79*	*−0.50*	*k*(3=4)(4−5)	*0.27*		*k*(C=C)(13′−Me)	0.20	
k(11=12)(13=14)	*−0.79*	*−0.70*	*k*(4−5)(5=6)	*0.27*		*k*(C−C)(C−Me)	0.20	
k(13=14)(15=15′)	*−0.75*	*−0.70*	*k*(5=6)(6−7)	*0.27*		*k*(C−C)(13−Me)	*0.10*	
k(15=15′)(13′=14′)	*−0.75*	*−0.60*	*k*(6−7)(7=8)	*0.27*		*k*(C−C)(13′−Me)	*0.10*	
k(13′=14′)(11′=12′)	*−0.50*	*−0.47*	*k*(7=8)(8−9)	*0.27*				
k(11′=12′)(9′=10′)	*−0.50*	*−0.47*	*k*(8−9)(9=10)	*0.30*	*0.38*	*h*(H−C=C)(C=C−H)	0.07	
k(2−3)(4−5)	−0.15		*k*(9=10)(10−11)	*0.30*	*0.38*	*h*(H−C11=C12)(C11=C12−H)	*0.076*	*−0.015*
k(4−5)(6−7)	−0.15		*k*(10−11)(11=12)	*0.30*	*0.38*	*h*(H−C15=C15′)(C15=C15′−H)	*0.05*	*0.11*
k(6−7)(8−9)	−0.15		*k*(11=12)(12−13)	*0.30*	*0.28*	*h*(H−C11′=C12′)(C11′=C12′−H)	*0.065*	*0.048*
k(8−9)(10−11)	*−0.02*	*−0.18*	*k*(12−13)(13=14)	*0.30*	*0.28*	*h*(H−C−C)(C−C−H)	0.09	
k(10−11)(12−13)	*−0.02*	*−0.18*	*k*(13=14)(14−15)	*0.13*	*0.28*	*h*(H−C10−C11)(C10−C11−H)	*0.09*	*0.16*
k(12−13)(14−15)	*−0.02*	*0.15*	*k*(14−15)(15=15′)	*0.13*	*0.00*	*h*(H−C14−C15)(C14−C15−H)	*0.085*	*−0.03*
k(14−15)(14′−15′)	*−0.15*	*0.10*	*k*(15=15′)(14′−15′)	*0.13*	*0.00*	*h*(H−C14′−C15′)(C14′−C15′−H)	*0.085*	*0.03*
k(14′−15′)(12′−13′)	*−0.04*	*−0.10*	*k*(14′−15′)(13′=14′)	*0.13*	*0.00*	*h*(H−C10′−C11′)(C10′−C11′−H)	*0.11*	*0.09*
k(12′−13′)(10′−11′)	*−0.04*	*−0.10*	*k*(13′=14′)(12′−13′)	*0.42*	*0.52*	*h*(H−C=C)(C=C−Me)	*0.03*	*0.0*
k(10′−11′)(8′−9′)	*−0.04*	*−0.10*	*k*(12′−13′)(11′=12′)	*0.42*	*0.52*			
k(10−11)(14−15)	*0.08*	*0.35*	*k*(11′=12′)(10′−11′)	*0.42*	*0.52*	*w*(C=C) trans	−0.005	
k(14′−15′)(10′−11′)	0.00	*−0.15*	*k*(10′−11′)(9′=10′)	*0.42*	*0.52*	*w*(C−C) trans	0.005	
k(12−13)(14′−15′)	*−0.10*	*0.00*	*k*(9′=10′)(8′−9′)	*0.42*	*0.52*			

[a] UBS force constants are abbreviated as follows: *K*, stretching; *H*, bending; *F*, nonbonded repulsion; *W*, out-of-plane wagging; *T*, torsion; and κ, intramolecular resistant force. The units of force constants are md·Å^{-1} for *K*, *H*, *F*, and κ, and md·Å for *W* and *T*. [b]Non-UBS cross terms include *k*, stretching-stretching; *h*, bending-bending; and *w*, wagging−wagging. The units are md•Å^{-1} for *k*, and md•Å for *h* and *w*. [c,d,e] Subscript "o" stands for the olefinic part, whereas subscripts "me" and "met" stand for the methyl and methylene parts, respectively. [f]Subscript "long" indicate long-range interaction with the next neighbor. Force constants shown in Roman were transferred or assumed, and those shown in italic were determined in the present investigation. Each blank in the column of the T_1 force constants indicates that the particular T_1 force constant was assumed to be the same as the S_0 force constant.

of modes taking place on both the left-hand-side and the right-hand-side is coupled in-phase with each other. In the T_1 state, on the other hand, the 1450 cm^{-1} Raman line is assigned to the 13Me asymmetric deformation and the 1006 cm^{-1} Raman line to the 9Me and 13Me rockings, both taking place on the left-hand-side.

Figure 5a shows the displacements of atoms in the C=C and C−C stretching modes giving rise to high Raman intensities; it supports the above idea. In the S_0 state, the 1529 cm^{-1} Raman line is due to the C11=C12, C13=C14, C13′=C14′ and C11′=C12′ stretchings coupled in-phase. Almost complete C_i symmetry is seen even for the coupled C−H ip bendings. The 1161 cm^{-1} Raman line is due to the C14−C15 and the C14′−C15′ stretchings that are coupled with the C15−H and the C15′−H ip bendings. Here again, C_i symmetry is clearly seen. In the T_1 state, on the other hand, the 1500 cm^{-1} Raman line is mainly due to the C13=C14 stretching and the 1165 cm^{-1} Raman line is due to the C10−C11 and the C14−C15 stretchings. Both normal modes are taking place on the left-hand-side of the C15=C15′ bond. This type of difference in normal modes reflect changes in the stretching force constants (bond orders) upon triplet excitation, the details of which will be discussed later.

(b) 15-cis-Spheroidene Bound to the RC. Twisting of the Conjugated Backbone in the S_0 and T_1 States. In a previous investigation, we compared the S_0 Raman spectrum of the RC-bound 15-*cis*-spheroidene to that of 15-*cis*-spheroidene free in *n*-hexane solution (see Figure 1 of ref 23). The weak

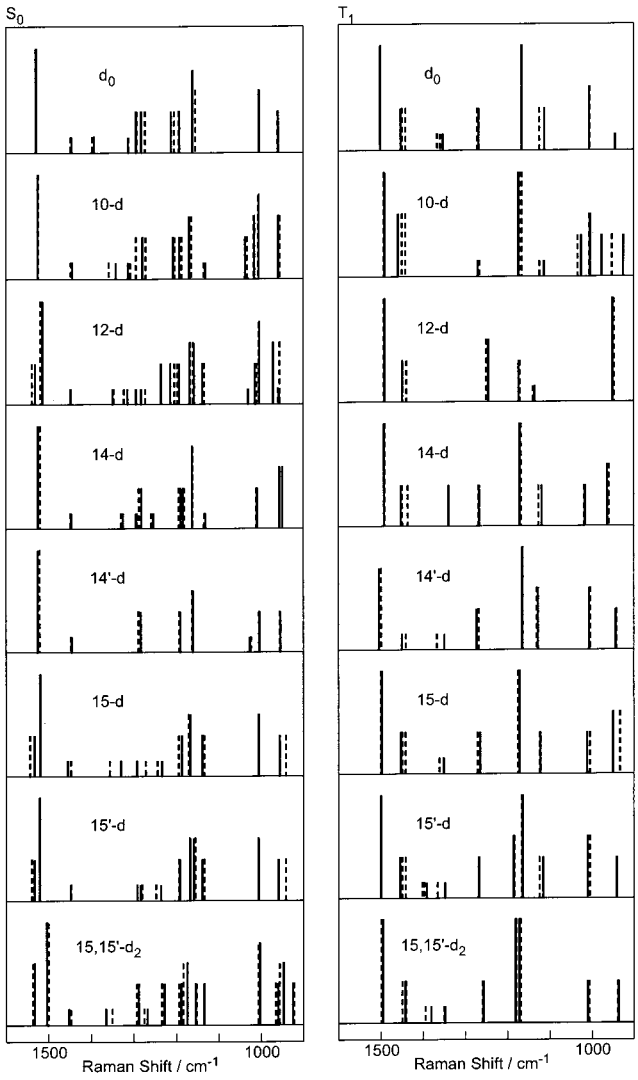

Figure 4. Comparison of observed and calculated frequencies for the S_0 and T_1 Raman lines of d_0 and various deuterio all-*trans*-spheroidenes in *n*-hexane solution. The observed Raman lines are roughly classified into four groups in intensity (very strong, strong, medium, and weak), and the observed and the calculated frequencies are shown in solid and broken Raman lines, respectively.

958 cm^{-1} Raman line in solution downshifted slightly and strongly enhanced upon binding to the RC to form the medium 954 cm^{-1} Raman line. The intensity enhancement was regarded as an indication of twisting around the C15═C15′ bond.[23] Because the assignment of the Raman line to the C15—H and C15′—H waggings coupled with the C15═C15′ torsion is now established in the present normal-coordinate analysis, and because test calculations showed that twisting causes the downshift of the particular Raman line, we temporarily estimated the twisting angle around the C15═15′ bond to be 30°.

As mentioned in a previous section, the T_1 Raman spectrum of the RC-bound 15-*cis*-spheroidene has suggested substantial twistings of the conjugated chain. The empirical and normal-coordinate analysis of the Raman spectrum shown in Figure 3 as well as test calculations to elucidate the effects of twisting around each C═C bond on the normal frequencies lead us to the following conclusions: (1) Twisting around the C15═C15′ bond: (i) The key Raman line of the 15-cis configuration at 1239 cm^{-1} in the S_0 state disappeared from this spectral region and shifted to as high as 1335 cm^{-1} in the T_1 state (the latter Raman line is more clearly seen in Figure 2 of ref 23). A set of normal-coordinate calculations showed that the twisting around the C15═C15′ bond causes decoupling of a pair of the C15—H and the C15′—H ip bendings from the C15═C15′ stretching, which naturally causes increase in frequency and decrease in intensity. (ii) The S_0 Raman line at 954 cm^{-1} with medium Raman intensity, which has been assigned to the C15—H and C15′—H waggings coupled with the C15═C15′ torsion, transforms into the T_1 Raman line at 935 cm^{-1} showing enormously high Raman intensity. This enhancement of the particular mode was ascribed to substantial twisting around the C15═C15′ bond.[23] Test normal-coordinate calculations showed that the twisting of the C15═C15′ bond (∼45°) causes substantial decrease in the above coupling, and as a result, low-frequency-shift of the particular mode. Further, the test calculations showed that the twisting around the C15═C15′ bond caused coupling of those "op" wagging mode with the "ip" type modes (the C13—Me and the C13′—Me stretching and the C14—C15═C15′ and the C15═C15′—C14′ bendings) to enhance the Raman intensity. (2) Twisting around the C11═C12 bond: (i) In the S_0 state, the C14—C15 and the C10—C11 stretchings appear at 1168 and 1159 cm^{-1}, whereas in the T_1 state, they appear at 1156 and 1182 cm^{-1}, respectively, with reversed order in frequency. Test normal-coordinate calculations indicated that the twisting around the C11═C12 bond (∼30°) causes decoupling among the ip vibrations including the C10—C11 stretching and the C11—H and C12—H bendings, and as a result, the high-frequency-shift of the particular stretching vibration. (ii) Upon the 15-d substitution of the RC-bound 15-*cis*-spheroidene in the T_1 state, the 935 cm^{-1} Raman line due to the C15—H and C15′—H waggings coupled with the C15═C15′ torsion disappears from this region. Then, two Raman lines appears in this region; one at 949 cm^{-1}, the C11—H and C12—H waggings coupled with the C11═C12 torsion, and the other at 921 cm^{-1}, the C15—D bending. The considerably high intensity of the former Raman line supports the twisting around the C11═C12 bond. (3) Twisting around the C13═C14 bond: (i) A pair of clearly-split Raman lines in the C═C stretching region is seen in the T_1 spectrum of the RC-bound spheroidene; one at 1526 cm^{-1} which has been assigned to the C11═C12 and the C11′═C12′ stretchings and the other at 1505 cm^{-1} which has been assigned to the C13═C14 stretching. Test calculations showed that the frequency of the latter mode downshifts when the C13═C14 bond is twisted (∼30°). Therefore, the widely split C═C stretching Raman lines indicate the twisting around the C13═C14 bond. It is also to be emphasized that such low frequency of the C13═C14 stretching mode could never be explained in terms of a stretching force constant when the value was similar to that determined for all-*trans*-spheroidene.

Taking into account all the results of the above test calculations, we estimated the twisting angles around the C15═C15′, C13═C14, and C11═C12 bonds to be +45°, −30°, +30°, respectively, in the case of the RC-bound 15-*cis*-spheroidene in the T_1 state. [We found that a model with the rotational angles (+45°, +30°, +30°) also explains the observed Raman data, a fact which indicates that decoupling of local vibrations on both sides of a particular twisted double bond is relevant to the spectral changes.] Those signs were chosen to minimize the change in the overall structure of the conjugated backbone and to fit the spheroidene molecule to the binding pocket (vide infra). The frequencies, the intensities and the normal modes of the relevant Raman lines do indicate the twisting around the C15═C15′, C13═C14, and C11═C12 bonds, but the twisting angles themselves are just a rough estimation that should not be taken too seriously.

TABLE 3: Frequencies of S_0 and T_1 Raman Lines and Frequencies and Normal Modes Calculated by Normal-Coordinate Analysis for (a) d_0 All-*trans*-Spheroidene in *n*-Hexane Solution and (b) d_0 15-*cis*-Spheroidene Bound to the RC

(a)	S_0 state		T_1 state		
obs	calc	assignment	obs	calc	assignment
1529	1530	C11═C12, C13═C14, C13′═C14′, C11′═C12′ str	1500	1500	C13═C14, C11═C12 str
1445	1447	13Me, 13′Me asym def	1450	1441	13Me asym def
1391	1396	13Me, 13′Me sym def			
1312	1310	C12─H, C12′─H bend	1352	1366	13Me sym def
1293	1293	C11′─H bend			
1281	1272	C11─H bend	1268	1271	C10─H, C12─H bend
1210	1204	C12─C13 str, C14─H bend			
		C12′─C13′ str, C14′─H bend			
1191	1193	C8─C9 str	1165	1165	C14─C15, C10─C11 str
		C10─H, C11─H bend			
1161	1161	C14─C15, C14′─C15′ str	1112	1124	C10─C11, C14─C15, C10′─C11′ str
	1154	C10─C11 str			
1004	1006	13Me, 13′Me rock	1006	1005	13Me, 9Me rock
959	960	C15─H, C15′─H wag, C15═C15′ tor	944	945	C15─H, C15′─H wag, C15═C15′ tor

(b)	S_0 state		T_1 state		
obs	calc	assignment	obs	calc	assignment
1534	1535	C13═C14, C11═C12, C13′═C14′, C11′═C12′ str	1526	1526	C11═C12, C11′═C12′ str
(1532)	1532	C15═C15′ str	1505	1505	C13═C14, C12─C13 str
1445	1447	13Me, 13′Me asym def			
1288	1296	C11′─H bend			
	1276	C11─H bend			
1239	1236	C15─H, C15′─H bend, C15═C15′ str	(1335)	1343	C12─C13, C12′─C13′ str
1212	1202	C12─C13, C12′─C13′ str			C15─H, C15′─H bend
		C14─H, C14′─H bend			
1190	1192	C8─C9 str, C10─H bend			
1168	1167	C14─C15 str	1182	1182	C10─C11 str
1159	1158	C10─C11 str	1156	1156	C14─C15 str
1001	1005	13Me, 13′Me rock	1008	1008	13Me, 9Me rock
973	965	C11─H, C12─H wag, C11═C12 tor			
954	953	C15─H, C15′─H wag, C15═C15′ tor	935	935	C15─H, C15′─H wag, C15═C15′ tor

Determination of Force Constants and Normal Modes. The S_0-state force constants for the RC-bound 15-*cis*-spheroidene were determined by the use of a model whose C15═C15′ cis bond is twisted by 30°. Then, normal-coordinate analysis was started by the use of force constants determined by Saito and Tasumi for 15-*cis*-β-carotene (for the central part)[46] and those determined for all-*trans*-spheroidene (the peripheral part). The number of independent force constants adjusted and the number of observed Raman lines used for fitting were 37 and 55, respectively.

In the T_1 state, the C10─C11, C11═C12, C12─C13, C13═C14, C14─C15, C15═C15′, and C13′═C14′ stretching force constants and the relevant cross terms alone were adjusted, assuming the twisting angles of +45°, −30°, and +30° around the C15═C15′, C13═C14, and C11═C12 bonds. The rest of the force constants were assumed to be the same as those determined in the S_0 state. As an initial guess, the above stretching force constants that were determined in T_1 all-*trans*-spheroidene in solution were transferred. Then, those force constants were adjusted to realize the observed Raman frequencies and the empirical assignments for all the RC-bound d_0 and deuterio 15-*cis*-spheroidenes in the T_1 state.

The results of normal-coordinate analysis for the S_0 and T_1 states of 15-*cis*-spheroidene bound to the RC can be summarized as follows: Table 4 lists the S_0 and T_1 force constants determined in the above normal-coordinate analysis (shown in italic). Table 3b lists the calculated frequencies and the normal modes for the d_0 species, which compare well to the observed Raman frequencies and the empirical assignments listed in Table 1b. (The calculated frequencies and the normal modes of various deuterio 15-*cis*-spheroidenes are given in Table 2S of "Supporting Information available".) Figure 6 depicts a comparison between the observed and the calculated frequencies for all the RC-bound d_0 and deuterio 15-*cis*-spheroidenes in both the S_0 and T_1 states, which proves the reliability of the set of force constants determined in the present normal-coordinate analysis. The C═C and the C─C stretching force constants will be used as a scale in the discussion of changes in bond orders upon triplet excitation.

Figure 5b characterizes the C═C and the C─C stretchings in the S_0 and T_1 states of 15-*cis*-spheroidene. In addition to the low-frequency-shift of the former and the high-frequency-shift of the latter in general, the following changes are seen upon triplet excitation. The C11═C12, C13═C14, C13′═C14′, and C11′═C12′ stretchings (1534 cm^{-1}) is overlapped with the C15═C15′ stretching (1532 cm^{-1}) to form a closely overlapped Raman line in the S_0 state, whereas the low-frequency-shift of the C13═C14 stretching (due to twisting around the C13═C14 bond) results in a pair of widely split Raman lines in the T_1 state (1526 and 1505 cm^{-1}). On the other hand, the C14─C15 stretching (1168 cm^{-1}) and the C10─C11 stretching (1159 cm^{-1}) form slightly split lines in the S_0 state, whereas a drastic high-frequency-shift of the latter (due to the twisting around the C11═C12 bond) causes a pair of widely split lines in the reversed order, i.e., the C10─C11 stretching (1182 cm^{-1}) and the C14─C15 stretching (1156 cm^{-1}) in the T_1 state. Those calculated frequencies and normal modes nicely reflect the twistings of the conjugated backbone around the C13═C14 and C11═C12 bonds.

Discussion

S_0- and T_1-State Bond Orders in the Conjugated Chain As Probed by Stretching Force Constants. *(a) All-trans-Spheroidene in Solution.* Figure 7a depicts the C═C and C─C stretching force constants in the S_0 and T_1 states which have

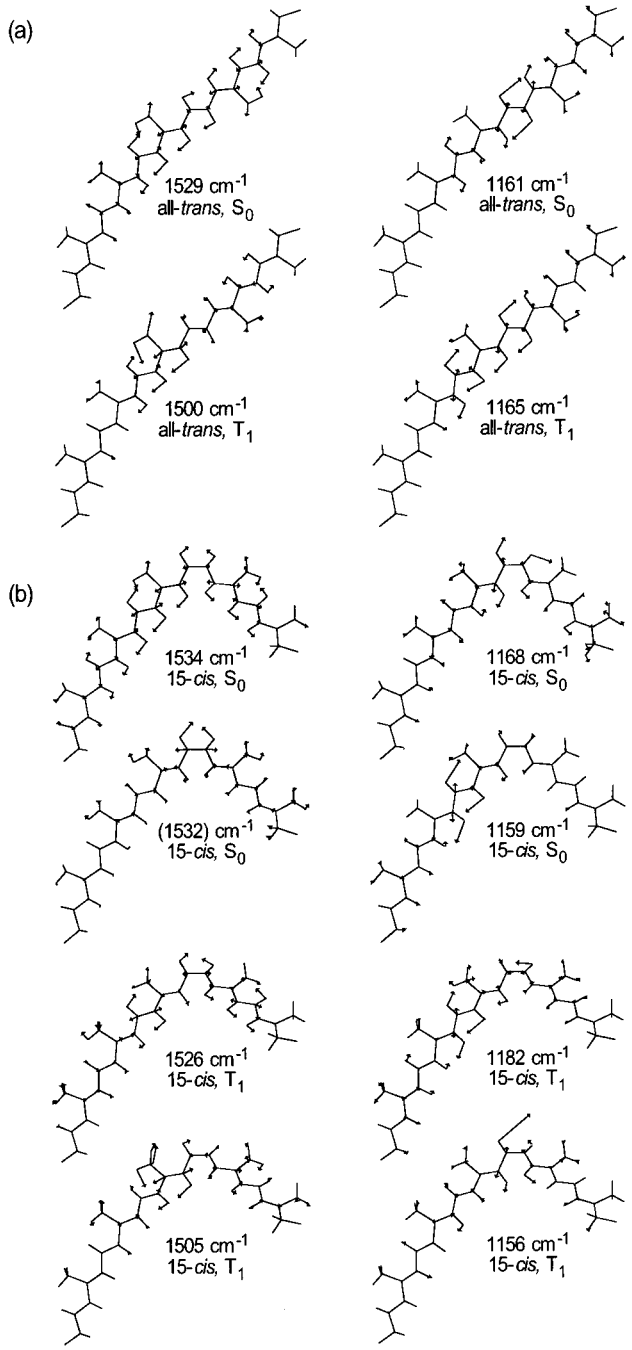

Figure 5. Comparison of normal modes among the prominent C═C and C−C stretching Raman lines in the S_0 and T_1 states for (a) d_0 all-*trans*-spheroidene in *n*-hexane solution and (b) d_0 15-*cis*-spheroidene bound to the RC.

been determined for all-*trans*-spheroidene free in *n*-hexane solution. Open circles indicate force constants in the S_0 state, whereas closed circles indicate those in the T_1 state. Now, we are going to discuss the carbon−carbon bond orders in the central part by the use of the set of stretching force constants as a scale. Before starting discussion, the unique chemical structure of the spheroidene molecule should be pointed out (see Figure 1a); the center of the entire carbon skeleton is located on the C15═C15′ bond, whereas the center of the conjugated chain on the C12−C13 bond.

In the S_0 state, the bond order of the C15═C15′ bond is the lowest among all the C═C bonds, and the bond order of neighboring bond increases toward both ends symmetrically with respect to the C15═C15′ bond. On the other hand, the bond order of the C−C bond exhibits a maximum around the C14−C15 and C14′−C15′ bonds. The symmetric changes in both carbon−carbon bond orders, with respect not to the center of the conjugated chain but to the C15═C15′ bond, obviously reflect the electronic structure influenced by the pair of methyl groups attached to the C13 and C13′ positions. Figure 8 compares, between all-*trans*-spheroidene and all-*trans*-β-carotene, the dependence of the ^{13}C chemical shift on the position of each carbon atom in the C11·····C11′ region. If we simply assume that those chemical-shift values reflect the electron densities on those carbon atoms, it can be concluded that the electronic structure in the particular region still reflects the symmetric influence of the pair of the 13 and 13′ methyl groups even in the case of the asymmetric carotenoid, all-*trans*-spheroidene, although it is not as perfect as the case of the symmetric carotenoid, all-*trans*-β-carotene. The shift of the center of the conjugated chain to the C12 and C13 atoms is also reflected as the asymmetry of the chemical-shift pattern with respect to the C15 and C15′ atoms.

In the T_1 state, on the other hand, the bond order of the C13═C14 bond is the lowest among all the C═C bonds, whereas that of the C12−C13 bond is the highest among the C−C bonds. Both the C═C and C−C bond orders tend to systematically change toward both terminals with respect to the center of the conjugated chain, i.e., the C12−C13 bond. If we focus our attention to changes in bond order upon triplet excitation, decrease in the C═C bond order is in the order, C13═C14 > C11═C12 > C9═C10 > C15═C15′, and increase in the C−C bond order is the largest in the C12−C13 bond. Those changes in bond orders are in good accord with the idea of "the triplet-excited region" we proposed previously (see refs 28, 31, and 49 for reviews). The triplet-excited region has been defined as a region where largest changes in bond order take place upon triplet excitation, i.e., double bonds become single bond-like, whereas single bonds become double bond-like. It has a span of approximately six conjugated double bonds, it is localized in the central part of a conjugated chain, and it triggers cis-to-trans isomerization in the T_1 state. It has been shown, in the present investigation, that the triplet-excited region is located in the center of the conjugated chain even in an asymmetric carotenoid, all-*trans*-spheroidene.

(b) 15-cis-Spheroidene Bound to the RC. Figure 7b shows the C═C and C−C stretching force constants in the S_0 and T_1 states that have been determined for the RC-bound 15-*cis*-spheroidene. Again, we are going to use the stretching force constants as a scale of bond orders. In the S_0 state, the bond order of the C15═C15′ bond is the lowest among all the C═C bonds, whereas the bond orders of the C14−C15 and the C14′−C15′ bonds are highest among all the C−C bonds. Approximately symmetric changes with respect to the C15═C15′ bond toward both ends of the conjugated chain are seen as in the case of all-*trans*-spheroidene in solution. In the T_1 state, on the other hand, the lowest bond order is seen for the C13═C14 bond among all the C═C bonds, and the highest bond order is seen for the C12−C13 bond among the C−C bonds. Upon triplet excitation, decrease in the C═C bond order is in the order, C13═C14 > C11═C12 > C15═C15′ (the C9═C10 stretching force constant could not be determined in this case), whereas increase in the C−C bond order is in the order, C12−C13 > C10−C11 > C14−C15. The magnitudes of changes in bond order upon triplet excitation in the RC-bound 15-*cis*-spheroidene tend to be larger than those in all-*trans*-spheroidene in solution, although the patterns of changes are very similar to each other.

TABLE 4: S_0 and T_1 Force Constants for 15-*cis*-Spheroidene Bound to the RC[a]

	S_0	T_1		S_0	T_1		S_0	T_1
Urey−Bradley−Shimanouchi (UBS) force constants								
K(Dy−C)	3.50		*K*(14−15)	*4.66*	*4.83*	*W*(HCC3═C)	0.335	
K(2−3)	3.80		*K*(15═15′)	*6.01*	*5.63*	*W*(HCC4═C)	0.335	
K(3═4)	6.70		*K*(14′−15′)	*4.63*		*W*(HCC6═C)	0.335	
K(4−5)	3.90		*K*(13′═14′)	*6.24*	*6.10*	*W*(HCC7═C)	0.335	
K(5═6)	6.60		*K*(12′−13′)	*4.39*		*W*(HCC8═C)	0.335	
K(6−7)	3.90		*K*(11′═12′)	*6.29*		*W*(HCC10═C)	0.33	
K(7═8)	6.50		*K*(10′−11′)	4.00		*W*(HCC11═C)	0.27	*0.246*
K(8−9)	*4.00*		*K*(9′═10′)	6.35		*W* (HCC12═C)	0.33	*0.306*
K(9═10)	*6.35*		*K*(8′−9′)	3.80		*W* (HCC14═C)	0.335	
K(10−11)	*4.36*	*4.72*	*K*(C−Me)	2.70		*W* (HCC15═C)	0.255	
K(11═12)	*6.23*	*5.64*	*K*(═CH) o	4.50		*W* (HCC15′═C)	0.255	
K(12−13)	*4.43*	*4.86*	*K*(−CH) me	4.27		*W* (HCC14′═C)	0.335	
K(13═14)	*6.20*	*5.47*	*K*(−CH) met	4.20		*W* (HCC12′═C)	0.33	
						W (HCC11′═C)	0.27	
H(C−C═C)	0.24		*F*(C−C═C)	0.34		*W* (HCC10′═C)	0.33	
H(C−C−C)	0.23		*F*(C−C−C)	0.40		*W* (MeCC═C)	0.335	
H(C═C−H)	0.205		*F*(C═C−H)	0.48				
H(C−C−H) o	0.20		*F*(C−C−H) o	0.41		*T*(C═C)	*0.485*	*0.458*
H(C−C−H) me	0.24		*F*(C−C−H) me	0.55		*T*(C−C)	0.09	
H(H−C−H) me	0.36		*F*(H−C−H) me	0.195		*T*(C−Me)	0.047	
H(Dy−C−C)	0.20		*F*(Dy−C−C)	0.40				
H(Dy−C−H)	0.19		*F*(Dy−C−H)	0.40				
H(C−C−H) met	0.19		*F*(C−C−H) met	0.40		κ me	−0.04	
H(H−C−H) met	0.40		*F*(H−C−H) met	0.10		κ met	−0.04	
non-UBS force constants								
k(3═4)(5═6)	−0.45		*k*(4−5)(5═6)	*0.39*		*k*(C−C)(13−Me)	0.20	
k(5═6)(7═8)	−0.45		*k*(5═6)(6−7)	*0.39*		*k*(C−C)(13′−Me)	0.20	
k(7═8)(9═10)	−0.45		*k*(6−7)(7═8)	*0.39*				
k(9═10)(11═12)	*−0.48*	*−0.30*	*k*(7═8)(8−9)	*0.39*		*h*(H−C═C)(C═C−H)	0.07	
k(11═12)(13═14)	*−0.48*		*k*(8−9)(9═10)	*0.40*	*0.10*	*h*(H−C11═C12)(C11═C12−H)	*0.026*	*0.03*
k(13═14)(15═15′)	*−0.34*	*−0.48*	*k*(9═10)(10−11)	*0.40*	*0.10*	*h*(H−C15═C15′)(C15═C15′−H)	*0.09*	
k(15═15′)(13′═14′)	*−0.34*	*−0.40*	*k*(10−11)(11═12)	*0.40*	*0.10*	*h*(H−C11′═C12′)(C11′═C12′−H)	*0.05*	
k(13′═14′)(11′═12′)	*−0.38*	*−0.37*	*k*(11═12)(12−13)	*0.40*	*0.44*	*h*(H−C−C)(C−C −H)	0.09	
k(11′═12′)(9′═10′)	*−0.38*	*−0.37*	*k*(12−13)(13═14)	*0.40*	*0.44*	*h*(H−C10−C11)(C10−C11−H)	*0.10*	
k(2−3)(4−5)	−0.15		*k*(13═14)(14−15)	*0.41*	*0.44*	*h*(H−C14−C15)(C14−C15−H)	*0.05*	*0.055*
k(4−5)(6−7)	−0.15		*k*(14−15)(15═15′)	*0.41*	*0.35*	*h*(H−C14′−C15′)(C14′−C15′−H)	*0.051*	
k(6−7)(8−9)	−0.15		*k*(15═15′)(14′−15′)	*0.41*	*0.35*	*h*(H−C10′−C11′)(C10′−C11′−H)	*0.12*	
k(8−9)(10−11)	*−0.07*		*k*(14′−15′)(13′═14′)	*0.41*	*0.35*	*h*(H−C═C)(C═C−Me)	*0.09*	*0.08*
k(10−11)(12−13)	*−0.07*		*k*(13′═14′)(12′−13′)	*0.49*	*0.60*			
k(12−13)(14−15)	*−0.07*	*−0.10*	*k*(12′−13′)(11′═12′)	*0.49*	*0.60*	*kh*(14−15)(15═15′−H)	*0.006*	*0.10*
k(14−15)(14′−15′)	*0.00*	*0.01*	*k*(11′═12′)(10′−11′)	*0.49*	*0.60*	*kh*(14′−15′)(15′═15−H)	*0.07*	*0.22*
k(14′−15′)(12′−13′)	*−0.15*		*k*(10′−11′)(9′═10′)	*0.49*	*0.60*	*kh*(14−15)(15′═15−H)	*0.074*	*0.20*
k(12′−13′)(10′−11′)	*−0.15*		*k*(9′═10′)(8′−9′)	*0.49*	*0.60*	*kh*(14−15)(13═14−H)	*0.005*	*−0.10*
k(10′−11′)(8′−9′)	*−0.15*		*k*(C═C)(C−C(Me)) long	*0.07*	*0.11*			
k(10−11)(14−15)	*−0.05*	*−0.10*	*k*(C═C)(C−Me)	0.20		*w*(C═C) trans	−0.005	
k(Dy−C)(C−C)	−0.15		*k*(C═C)(13−Me)	0.20		*w*(C−C) trans	0.005	
k(2−3)(3═4)	*0.39*		*k*(C═C)(13′−Me)	0.20	*0.30*	*w*(C═C) cis	−0.063	
k(3═4)(4−5)	*0.39*		*k*(C−C)(C−Me)	0.20				

[a] See the foot notes of Table 2.

If one assumes a linear relation between the carbon−carbon bond length and the stretching force constant, a change of 1 md·Å^{-1} in force constant corresponds to a change of 0.064 Å in bond length. Then, increase in the bond length of the C13═C14 bond upon triplet excitation, for example, can be estimated to be 0.04 and 0.05 Å in all-*trans*-spheroidene in *n*-hexane solution and 15-*cis*-spheroidene in the RC, respectively.

Rotational Motions around the C15═C15′, C13═C14, and C11═C12 Bonds As a Mechanism of Triplet-Energy Dissipation. Resonance-Raman spectroscopy and normal-coordinate analysis of the RC-bound d_0 and various deuterio spheroidenes have provided us with structural information concerning the T_1-state spheroidene in the RC: (1) Large changes in bond order upon triplet excitation have been identified in the central part of the conjugated chain. The lengthenings of the C13═C14, C11═C12, and C15═C15′ bonds have been estimated to be 0.05, 0.04, and 0.02 Å, respectively. (2) Twisting of the conjugated chain around the C15═C15′, C13═C14, and C11═C12 bonds, by approximately +45°, −30°, and +30°, have been identified in the T_1 state, whereas twisting around the C15═C15′ bond alone by 30° has been found in the S_0 state. The above structural changes in the RC upon triplet excitation must originate from the binding pocket of the apo-protein and the intrinsic T_1-state properties of the chromophore, spheroidene. Actually, close examination of the X-ray structures of the RC-bound 15-*cis*-spheroidene (in the S_0 state) and the binding pocket revealed that the left-hand-side of the spheroidene molecule shown in Figure 1a is in close contact with the M subunit, the macrocycle of one of the accessory bacteriochlorophylls and the phytyl chain of one of the special-pair bacteriochlorophylls.[50] Therefore, the alternate signs of rotational angles around the *cis*-C15═C15′, *trans*-C13═C14 and trans C11═C12 bonds (+45°, −30°, +30°) must become necessary even after triplet excitation. On the other hand, the right-hand-side of the molecule is in weak contact with the M subunit, allowing the rotational degree of freedom of this branch.

As an intrinsic property, 15-*cis*-spheroidene in solution rapidly isomerizes into all-*trans*-spheroidene upon triplet excitation, and

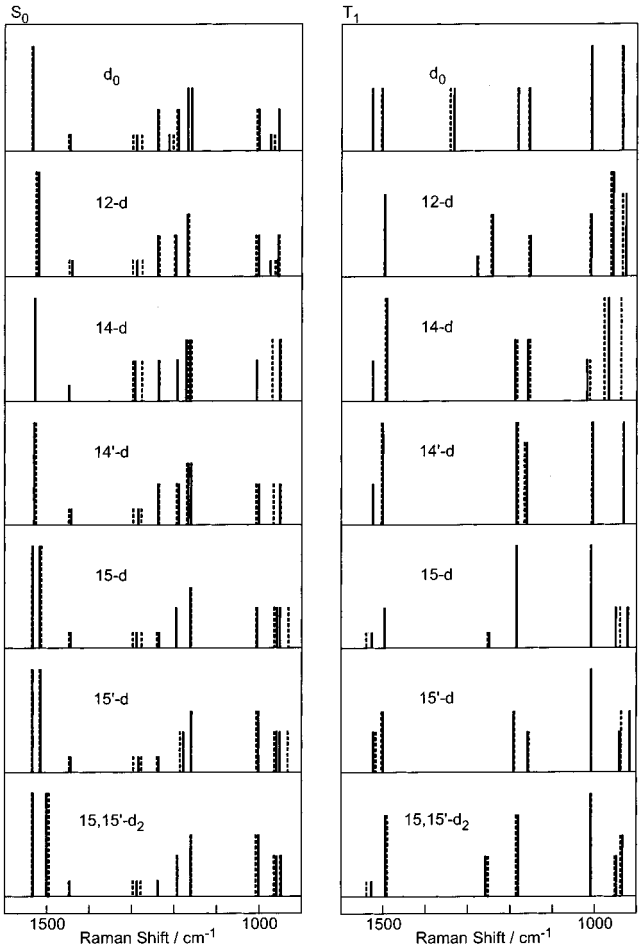

Figure 6. Comparison of observed and calculated frequencies for the S_0 and T_1 Raman lines of d_0 and various deuterio 15-*cis*-spheroidenes bound to the RC. The observed Raman lines are roughly classified into four groups in intensity (very strong, strong, medium and weak), and the observed and the calculated frequencies are shown in solid and broken lines, respectively.

therefore, it is not straightforward to apply resonance-Raman spectroscopy to the former to elucidate its T_1-state structure. However, changes in bond order, basically the same as all-*trans*-spheroidene, are expected to take place upon triplet excitation to trigger the isomerization reaction, which is presumably caused by the steric hindrance on the concave side of the 15-*cis*-bent structure.

Time-resolved absorption spectroscopy has been applied to isomeric spheroidenes in solution to elucidate the unique T_1-state properties of the 15-*cis*-isomer:[33] (1) The $T_1 \rightarrow S_0$ intersystem crossing takes place much faster in "*cis*-T_1" (0.83 μs) than in "all-*trans*-T_1" (4.76 μs). (2) The T_1-state isomerization from "*cis*-T_1" to "all-*trans*-T_1" takes place with efficiency in the order, "15-*cis*-T_1" (0.56 μs) > "13-*cis*-T_1" (0.77 μs) > "9-*cis*-T_1" (0.83 μs) > "13′-*cis*-T_1" (0.91 μs). (3) The quantum yield of triplet-sensitized isomerization (per triplet species generated) was determined to be 15-cis (0.60) > 13-cis (0.52) > 9-cis (0.50) > 13′-cis (0.48). The above results show that 15-*cis*-spheroidene is most advantageous over all the other *cis*−*trans* spheroidenes in dissipating the triplet energy through rotation around the cis bond (see the Introduction section). The following excited-state dynamics is expected to take place upon triplet excitation of 15-*cis*-spheroidene free in solution. First, decrease in the bond order of the C15═C15′ bond should take place to reduce the barrier against isomerization. Then, "15-*cis*-T_1" is supposed to have two routes for relaxation down to

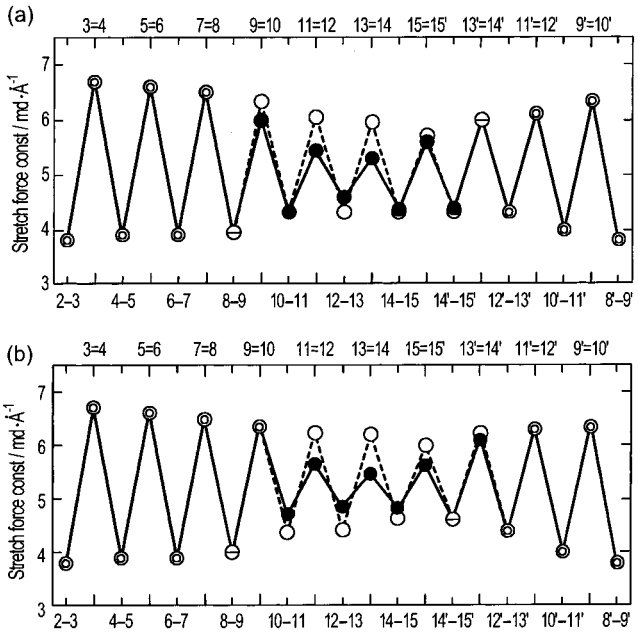

Figure 7. Comparison of the carbon−carbon stretching force constants determined in the S_0 state (open circles) and the T_1 state (closed circles) for (a) all-*trans*-spheroidene in *n*-hexane solution and (b) 15-*cis*-spheroidene bound to the RC. Double open circles indicate those stretching force constants which were assumed and could not be determined because of the limited number of deuterio species and/or the lack of observed Raman lines due to the normal modes in the peripheral parts. Lined open circles indicate complete overlap of the open and double open circles.

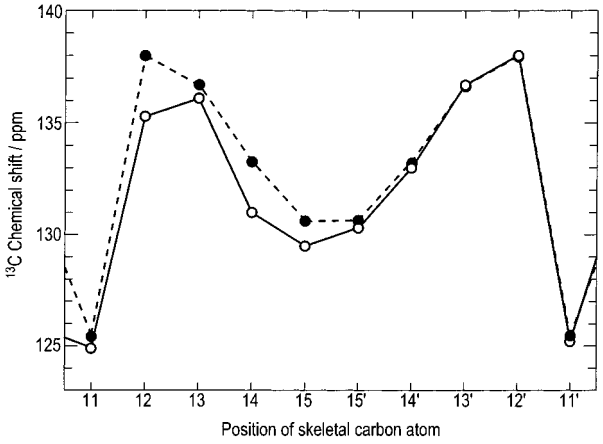

Figure 8. Dependence of ^{13}C chemical shift on the position of skeletal carbon atom in the central part. Open circles indicate the ^{13}C chemical shifts for all-*trans*-spheroidene and closed circles those for all-*trans*-β-carotene.

the S_0 state. Route A: to directly intersystem cross down to 15-*cis*-S_0 in submicroseconds (0.83 μs). Route B: to isomerize into "all-*trans*-T_1" in submicroseconds (0.56 μs), and then, to intersystem cross from "the resultant all-*trans*-T_1" to all-*trans*-S_0 in the microsecond time scale (4.76 μs). It is worthy of note that the time scale of $T_1 \rightarrow S_0$ intersystem crossing for the *cis*-T_1 species (0.83 μs) is in the same order as that of the T_1-state isomerization of *cis*-spheroidenes (0.56−0.91 μs). The result strongly supports the idea that the rotational motion around the C═C bond strongly enhances the $T_1 \rightarrow S_0$ intersystem crossing. This relation can be easily understood because the rotational motion causes a change in the orbital angular momentum (the electronic structure of the relevant carbon atoms changes from the sp^2 to the sp^3 type), and as a result, it causes change in the

spin angular momentum conserving the total angular momentum[51] (see the Introduction section).

The above considerations lead us to call Route A "a fast process of intersystem crossing through rotational motion", which is an intrinsic property of the T_1-state 15-*cis*-spheroidene. On the other hand, we call the latter part of Route B "a slow process of intersystem crossing in a fixed conformation", because "all-*trans*-T_1" has no further momentum of rotational motion to isomerize. [Fluctuation around the most stable rotational angle(s) may facilitate the intersystem crossing through the spin−orbit coupling mentioned above.] Now, we are going to apply the idea of the slow and fast processes of intersystem crossing to the case of the RC-bound spheroidene.

In the case of 15-*cis*-spheroidene in the RC, the first part of Route B, i.e., complete isomerization to "all-*trans*-T_1", is prohibited. Raman spectroscopy has shown that the twistings around the conjugated double bonds take place not only around the C15═C15′ bond but also around the C13═C14 and the C11═C12 bonds in "the triplet-excited region". Here, the rotational angles of +45°, −30°, +30° must be determined as the above-mentioned balance between the rotational momentum around the C15═C15′ bond (toward all-trans) vs the steric hindrance originating from the binding pocket of the apo-protein. After reaching this stationary-state twisted conformation in the T_1 state, only "the slow process of intersystem crossing in a fixed conformation" can take place, because no rotational degrees of freedom to enhance the intersystem crossing are left in this equilibrium configuration. The situation is similar to the case of "all-*trans*-T_1" free in solution.

On the other hand, the rotational motions around the 15═15′ double bonds which is supposed to take place immediately after triplet excitation (before reaching the above stationary-state T_1 structure) must strongly enhance the intersystem crossing down to the S_0-state, the mechanism of which should be similar to the case of 15-*cis*-spheroidene in solution. This corresponds to "the fast process of intersystem crossing through rotational motion" defined above. This type of rotational motion around the C15═C15′ bond within the 15-cis potential minimum has already been proposed as a mechanism of triplet-energy dissipation (see Figure 5 of ref 23). The present results show that this mechanism may need to be revised by adding the rotational motions around the C13═C14 and C11═C12 bonds as well, both under the influence of the trans potential minima.

Our hypothetical mechanism of triplet-energy dissipation initiated by the rotational motion around the *cis*-C15═C15′ bond has been questioned by some investigators: Specifically, (1) Bautista et al. [36] incorporated locked 15-*cis*-spheroidene, the configuration of which was chemically locked into 15-cis, into the RC of a carotenoidless mutant of *Rb. sphaeroides* R26.1, and determined the T_1 decay time constant to be 7 ± 1 μs. This value was not substantially larger than that of unlocked 15-*cis*-spheroidene in the RC, i.e., 4−5 μs [4] or $5 \pm 2 \approx 7.2 \pm 1$ μs (presented in the abstract and Table 1 of ref 9). Bautista et al.[36] took the result as evidence for that locked 15-*cis*-spheroidene is as capable of quenching the primary donor triplet as the unlocked spheroidene. (2) The observation that the T_1 lifetime of the LH2-bound all-*trans*-spheroidene, i.e., 7 μs,[52] is not very different from that of the RC-bound spheroidene, i.e., 4−5 μs, has also been taken as evidence against the hypothetical mechanism.[53]

Those observations can be nicely explained when one regards all the above decay time constants as representing "the slow process of intersystem crossing in a fixed conformation". When the rotational motion (toward "all-*trans*-T_1") is prohibited either by being buried in the binding pocket (4−5 μs) or by locking by the use of chemical bonds (7 μs), the decay time constant of such T_1 15-*cis*-spheroidene is in a similar order of magnitude to that of T_1 all-*trans*-spheroidene in solution (4.76 μs) or bound to the LH2 complex (7 μs). It is worthy of note that the chemically locked 15-*cis*-spheroidene tends to decay more slowly (7 μs) than unlocked 15-*cis*-spheroidene (4−5 μs), and that all-*trans*-spheroidene bound to the LH2 complex (7 μs) decays more slowly than that free in solution (4.76 μs). Those trends suggest that the rotational degree of freedom causing the fluctuation of rotational angles "in a fixed conformation" is an important factor even in "the slow process of intersystem crossing".

To fully understand the reason for the natural selection of the 15-cis configuration by the RC, and to establish the mechanism of triplet-energy dissipation, it is absolutely necessary to experimentally identify the fast process of intersystem crossing and the rotational motion in the submicrosecond (or even shorter) time range in the RC-bound 15-*cis*-spheroidene. A quantitative analysis of time-dependent changes in the triplet population in this time scale by EPR spectroscopy as well as the detection of the initial rotational motions by time-resolved absorption or Raman spectroscopy may provide us with a strong support for the present, more specific hypothetical mechanism of triplet-energy dissipation.

Acknowledgment. The authors are indebted to Prof. Harry Frank for transferring to them the technique of incorporating spheroidene into the carotenoidless RC. Financial supports from the Science Research Promotion Fund and from the Japan Society for the Promotion of Science are gratefully acknowledged. R.F. has been supported by a JSPS fellowship for Japanese junior scientists, and a grant-in-aid from the Ministry of Education, Science, Sports and Culture, Japan (# 7725).

Supporting Information Available: Table 1S: Frequencies of S_0 and T_1 Raman Lines and Frequencies and Normal Modes Calculated by Normal-Coordinate Analysis for Various Deuterio All-*trans*-Spheroidene in *n*-Hexane Solution, and Table 2S: Frequencies of S_0 and T_1 Raman Lines and Frequencies and Normal Modes Calculated by Normal-Coordinate Analysis for Various Deuterio 15-*cis*-Spheroidene Bound to the RC. This material is available free of charge via the Internet at http://pubs.acs.org.

References and Notes

(1) Frank, H. A.; Cogdell, R. J. *Carotenoids in Photosynthesis*, 1st ed.; Chapman & Hall: London, 1993; Chapter 8.

(2) Koyama, Y. *J. Photochem. Photobiol. B: Biol.* **1991**, *9*, 265.

(3) Frank, H. A. *The Photosynthetic Reaction Center Vol. II*; Deisenhofer, J., Norris, J. R. Eds., Academic Press: San Diego, 1993; Chapter 9.

(4) Cogdell, R. J.; Monger, T. G.; Parson, W. W. *Biochim. Biophys. Acta* **1975**, *408*, 189.

(5) Shuvalov, V. A.; Parson, W. W. *Proc. Natl. Acad. Sci. U.S.A.* **1981**, *78*, 957.

(6) Shuvalov, V. A.; Parson, W. W. *Biochim. Biophys. Acta* **1981**, *638*, 50.

(7) Schenck, C. C.; Mathis, P.; Lutz, M. *Photochem. Photobiol*. **1984**, *39*, 407.

(8) Frank, H. A.; Violette, C. A. *Biochim. Biophys. Acta* **1989**, *976*, 222.

(9) Frank, H. A.; Chynwat, V.; Posteraro, A.; Hartwich, G.; Simonin, I.; Scheer, H. *Photochem. Photobiol.* **1996**, *64*, 823.

(10) Frank, H. A.; Machnicki, J.; Friesner, R. *Photochem. Photobiol.* **1983**, *38*, 451.

(11) Hartwich, G.; Scheer, H.: Aust, V.; Angerhofer, A. *Biochim. Biophys. Acta* **1995**, *1230*, 97.

(12) Lutz, M.; Kleo, J.; Reiss-Husson, F. *Biochem. Biophys. Res. Com*. **1976**, *69*, 711.
(13) Koyama, Y.; Kito, M.; Takii, T.; Saiki, K.; Tsukida, K.; Yamashita, J. *Biochim. Biophys. Acta* **1982**, *680*, 109.
(14) Koyama, Y.; Takii, T.; Saiki, K.; Tsukida, K. *Photobiochem. Photobiophys.* **1983**, *5*, 139.
(15) Boucher, F.; van der Rest, M.; Gingras, G. *Biochim. Biophys. Acta* **1977**, *461*, 339.
(16) Lutz, M.; Szponarski, W.; Berger, G.; Robert, B.; Neumann, J.-M. *Biochim. Biophys. Acta* **1987**, *894*, 423.
(17) Gebhard, R.; van der Hoef, K.; Violette, C. A.; de Groot, H. J. M.; Frank, H. A.; Lugtenburg, J. *Pure Appl. Chem.* **1991**, *63*, 115.
(18) de Groot, H. J. M.; Gebhard, R.; van der Hoef, I.; Hoff, A. J.; Lugtenburg, J. *Biochemistry* **1992**, *31*, 12 446.
(19) Yeates, T. O.; Komiya, H.; Chirino, A.; Rees, D. C.; Allen, J. P.; Feher, G. *Proc. Natl. Acad. Sci. U.S.A.* **1988**, *85*, 7993.
(20) Arnoux, B.; Gaucher, J.-F.; Ducruix, A.; Reiss-Husson, F. *Acta Crystallogr., Sect. D* **1995**, *51*, 368. PDB 1YST.
(21) Koyama, Y.; Kanaji, M.; Shimamura, T. *Photochem. Photobiol*. **1988**, *48*, 107.
(22) Kok, P.; Köhler, J.; Groenen, E. J. J.; Gebhard, R.; van der Hoef, I.; Lugtenburg, J.; Hoff, A. J.; Farhoosh, R.; Frank, H. A. *Biochim. Biophys. Acta* **1994**, *1185*, 188.
(23) Ohashi, N.; Ko-chi, N.; Kuki, M.; Shimamura, T.; Cogdell, R. J.; Koyama, Y. *Biospectroscopy* **1996**, *2*, 59.
(24) Koyama, Y.; Takatsuka, I., Kanaji, M.; Tomimoto, K.; Kito, M.; Shimamura, T.; Yamashita, J.; Saiki, K.; Tsukida, K. *Photochem. Photobiol.* **1990**, *51*, 119.
(25) Bialek-Bylka, G. E.; Tomo, T.; Satoh, K.; Koyama, Y. *FEBS Lett.* **1995**, *363*, 137.
(26) Bialek-Bylka, G. E.; Fujii, R.; Chen, C.-H.; Oh-oka, H.; Kamiesu, A.; Satoh, K.; Koike, H.; Koyama, Y. *Photosyn. Res.* **1998**, *58*, 135.
(27) Bialek-Bylka, G. E.; Hiyama, T.; Yumoto, K.; Koyama, Y. *Photosyn. Res.* **1996**, *49*, 245.
(28) Koyama, Y.; Fujii, R. *The Photochemistry of Carotenoids*; Frank, H. A.; Young, A. J.; Britton, G.; Cogdell, R. J., Eds.; Kluwer Academic Publishers: Dordrecht, 1999; Chapter 9.
(29) Hashimoto, H.; Koyama, Y. *J. Phys. Chem*. **1988**, *92*, 2101.
(30) Hashimoto, H.; Koyama, Y.; Ichimura, K.; Kobayashi, T. *Chem. Phys. Lett.* **1989**, *162*, 517.
(31) Kuki, M.; Koyama, Y.; Nagae, H. *J. Phys. Chem*. **1991**, *95*, 7171.
(32) Koyama, Y.; Mukai, Y. *Biomolecular Spectroscopy, Part B*; Clark, R. J. H.; Hester, R. E. Eds., Wiley & Sons Ltd.: Chichester, 1993; Chapter 2.
(33) Fujii, R.; Furuichi, K.; Zhang, J.-P.; Nagae, H.; Hashimoto, H.; Koyama, Y. *J. Phys. Chem.* A, in press.
(34) Koyama, Y. *Carotenoid: Chemistry and Biology*; Krinsky, N. I., Mathews-Roth, M. M., Taylor, R. F. Eds., Plenum Press: New York, 1990; p 207.
(35) Lutz, M.; Chinsky, L.; Turpin, P.-Y. *Photochem. Photobiol*. **1982**, *36*, 503.
(36) Bautista, J. A.; Chynwat, V.; Cua, A.; Jansen, F. J.; Lugtenburg, J.; Grosztola, D.; Wasielewski, M. R.; Frank, H. A. *Photosynth. Res*. **1998**, *55*, 49.
(37) Kok, P.; Köhler, J.; Groenen, E. J. J.; Gebhard, R.; van der Hoef, I.; Lugtenburg, J.; Farhoosh, R.; Frank, H. A. *Spectrochimica Acta Part A* **1997**, *53*, 381.
(38) Jiang, Y.-H.; Kurimoto, Y.; Shimamura, T.; Ko-chi, N.; Ohashi, N.; Mukai, Y.; Koyama, Y. *Biospectroscopy* **1996**, *2*, 47.
(39) Gebhard, R.; van Dijk, J. T. M.; Boza, M. V. T. J.; van der Hoef, K.; Lugtenburg, J. *Recl. Trav. Chim. Pays-Bas* **1991**, *110*, 332.
(40) Cogdell, R. J.; Parson, W. W.; Kerr. M. A. *Biochim. Biophys. Acta* **1976**, *430*, 83.
(41) Frank, H. A.; Chunwat, V.; Hartwich, G.; Meyer, M.; Katheder, I.; Scheer, H. *Photosyn. Res.* **1993**, *37*, 193.
(42) Limantara, L.; Fujii, R.; Zhang, J.-P.; Kakuno, T.; Hara, H.; Kawamori, A.; Yagura, T.; Cogdell, R. J.; Koyama, Y. *Biochemistry* **1998**, *37*, 17 469.
(43) Sterling, C. *Acta Crystallogr*. **1964**, *17*, 1224.
(44) Wilson, E. B., Jr.; Decius, J. C.; Cross, P. C. *Molecular Vibrations The Theory of Infrared and Raman Vibrational Spectra*; McGraw-Hill Book Company, Inc.: New York, 1955.
(45) Shimanouchi, T. *Computer Programs for Normal Coordinate Treatment of Polyatomic Molecules*; University of Tokyo: Tokyo, 1968.
(46) Saito, S.; Tasumi, M. *J. Raman Spectrosc.* **1983**, *14*, 310.
(47) Koyama, Y.; Takatsuka, I.; Nakata, M.; Tasumi, M. *J. Raman Spectrosc.* **1988**, *19*, 37.
(48) Mukai, Y.; Abe, M.; Katsuta, Y.; Tomozoe, S.; Ito, M.; Koyama, Y. *J. Phys. Chem.* **1995**, *99*, 7160.
(49) Koyama, Y.; Mukai, Y.; Kuki, M. *SPIE Laser Spectroscopy of Biomolecules*, **1992**, *1921*, 191.
(50) McAuley, K. E.; Fyte, P. K.; Ridge, J. P.; Cogdell, R. J.; Isaacs, N. W.; Jones, M. R. *Biochemistry* **2000**, *39*, 15 032.
(51) Turro, N. J. *Modern Molecular Photochemistry*; The Benjamin/Cummings Publishing Co., Inc.: Menlo Park, 1978; Chapter 5.
(52) Monger, T. G.; Cogdell, R. J.; Parson, W. W. *Biochim. Biophys. Acta* **1976**, *449*, 136.
(53) Richard Cogdell, personal communication.